

# Enantioselective Anion Recognition by Chiral Halogen Bonding [2]Rotaxanes

Jason Y. C. Lim<sup>a</sup>, Igor Marques<sup>b,c</sup>, Vítor Félix<sup>b,c</sup> and Paul D. Beer<sup>a,\*</sup>

<sup>a</sup> Chemistry Research Laboratory, Department of Chemistry, University of Oxford, Mansfield Road, Oxford, OX1 3TA (UK). Email: [paul.beer@chem.ox.ac.uk](mailto:paul.beer@chem.ox.ac.uk). <sup>b</sup> Department of Chemistry, CICECO – Aveiro Institute of Materials, University of Aveiro, 3810-193 Aveiro, Portugal. <sup>c</sup> Department of Medical Sciences, iBiMED – Institute of Biomedicine, University of Aveiro, 3810-193 Aveiro, Portugal.

**ABSTRACT:** The application of chiral interlocked host molecules for discrimination of guest enantiomers has been largely overlooked, which is surprising given their unique three-dimensional binding cavities capable of guest encapsulation. Herein, we combined the stringent linear geometric interaction constraints of halogen bonding (XB), the non-covalent interaction between an electrophilic halogen atom and a Lewis base, with highly preorganized and conformationally restricted chiral cavities of [2]rotaxanes to achieve enantioselective anion recognition. Representing the first detailed investigation of the use of chiral XB rotaxanes for this purpose, extensive <sup>1</sup>H NMR binding studies and molecular dynamics (MD) simulation experiments revealed that the chiral rotaxane cavity significantly enhances enantio-discrimination compared to the non-interlocked free axle and macrocycle components. Furthermore, by examining the enantioselectivities of a family of structurally similar XB [2]rotaxanes containing different combinations of chiral and achiral macrocycle and axle components, the dominant influence of the chiral macrocycle in our rotaxane design for determining the effectiveness of chiral discrimination is demonstrated. MD simulations reveal the crucial geometric roles played by the XB interactions in orientating the bound enantiomeric anion guests for chiral selectivity, as well as the critical importance of the anions' hydration shells in governing binding affinity and enantio-discrimination.

## INTRODUCTION

Stimulated by the exceptional levels of enantioselectivity found in biotic systems, supramolecular chiral recognition, the ability of a chiral host molecule to selectively bind one guest enantiomer over the other, has witnessed a surge in interest in recent years, driving advances in analytical chemistry,<sup>1–3</sup> drug analysis,<sup>4</sup> asymmetric synthesis and catalysis.<sup>5–9</sup> In nature, guest enantiomer selectivity occurs via structurally well-defined binding pockets capable of encapsulating the target guest enantiomer in three-dimensional chiral cavities with exquisite complementarity.<sup>10</sup> Indeed, the importance of guest encapsulation in the chiral discrimination process has been demonstrated by the high levels of selectivity attained by abiotic receptors possessing structurally-enclosed chiral cavities in the form of macrocycles<sup>11–15</sup> and cryptand-like strapped calixpyrroles.<sup>16</sup> In this respect, the preorganized cavities of mechanically-interlocked molecules (MIM) such as rotaxanes and catenanes offer unique opportunities for enantioselective

discrimination when judiciously decorated with chiral functionalities. Although MIMs have been successfully exploited for the recognition of charged guest species,<sup>17–19</sup> in particular anions,<sup>20–22</sup> their potential for chiral guest recognition has been largely overlooked,<sup>23</sup> which may be a consequence of the challenging synthesis of chiral MIMs. However, recent years have witnessed significant advancements in their synthetic methodologies<sup>24–30</sup> most notably via metal template protocols.<sup>31–35</sup> Rare examples of chiral binding studies involving MIMs to date include a qualitative investigation with a racemic mechanically bonded-chiral rotaxane<sup>36</sup> and recently, a chiral catenane which exhibits modest discrimination between cationic chiral diamines.<sup>34</sup> To the best of our knowledge, chiral recognition by rotaxane host systems has yet to be studied in detail.

Amongst the non-covalent interactions employed in solution-phase chiral discrimination, halogen bonding (XB), the highly directional interaction resulting from the sigma hole of an electron-deficient halogen atom and a

Lewis base,<sup>37–39</sup> remains virtually unexploited.<sup>40,41</sup> We have recently demonstrated the enhanced enantioselective recognition properties of chiral anions by acyclic chiral XB host molecules compared to their hydrogen bonding (HB) analogues.<sup>42,43</sup> Herein, we describe the integration of XB-donor groups into a chiral macrocycle,<sup>44</sup> and by using an active metal template approach, into unprecedented chiral XB [2]rotaxane host structural frameworks. Importantly, we demonstrate a XB rotaxane containing both chiral axle and macrocycle units exhibits notably enhanced chiral discrimination properties compared to its free components. By comparing the enantioselective anion binding properties of structurally-related XB [2]rotaxanes containing different combinations of chiral and achiral macrocycle and axle components (Chart 1), we also show that the chiral macrocycle unit was the main contributor to the overall enantioselective recognition process. Furthermore, molecular dynamics (MD) simulations carried out in wet organic media highlight the crucial geometric roles played by XB interactions and the importance of enantiomer anion substrate hydration in determining the experimentally observed enantioselectivities.

## RESULTS AND DISCUSSION

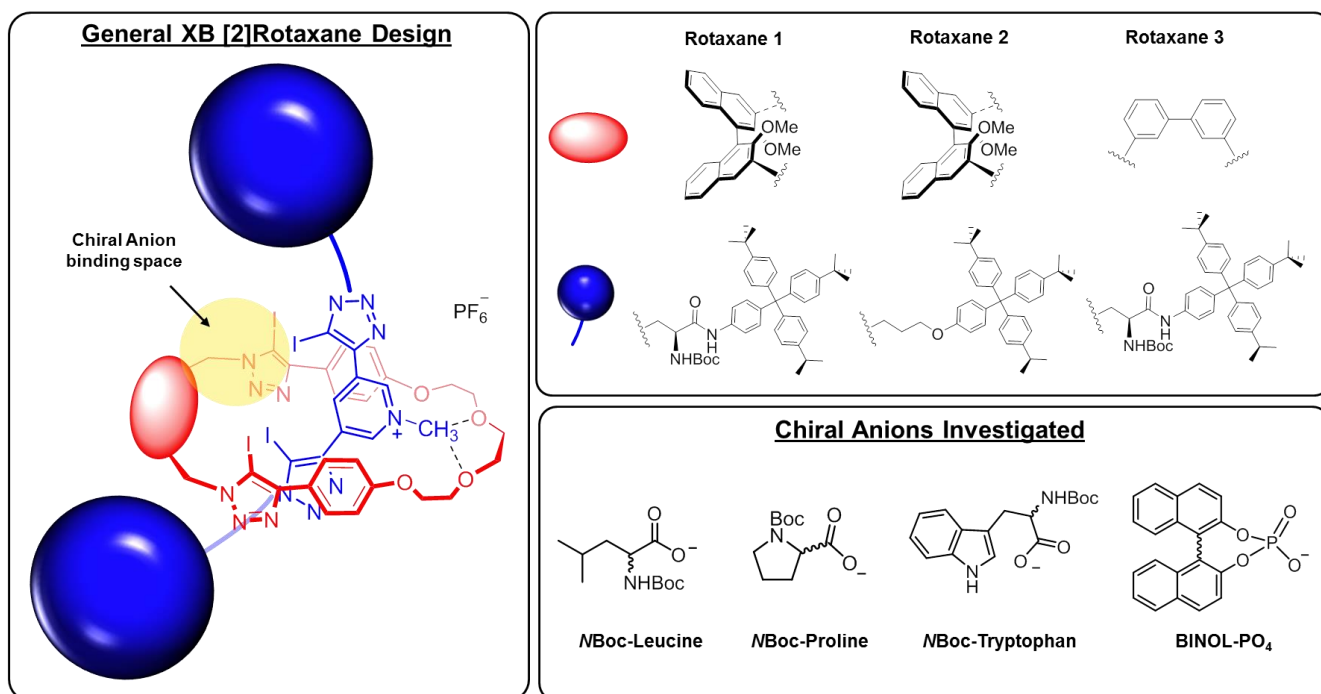
**Design and Syntheses of Chiral XB [2]Rotaxanes.** Due to its rigidity, stable chiral configuration and ease of chemical functionalisation,<sup>45</sup> the chiral (*S*)-1,1'-bi-2-naphthol (BINOL) motif was incorporated into the design of the XB macrocycle component of [2]rotaxane **1** (Chart 1). A methylene spacer inserted between the (*S*)-BINOL and iodotriazole XB-donor motifs allows sufficient flexibility for strong anion binding by convergent XB interactions, while maintaining the necessary rigidity and close proximity to the chiral (*S*)-BINOL motif for chiral discrimination.<sup>42</sup> Rotaxane **1** also contains a chiral 3,5-bis-iodotriazole pyridinium axle component derived from enantio-pure (*S*)-serine that threads through the macrocycle cavity.<sup>46</sup> As shown in Chart 1, hydrogen bonding interactions between the pyridinium methyl group of the axle and the polyether region of rotaxane **1**'s macrocycle component is expected to lock both components rigidly together,<sup>47–49</sup> sandwiching the chiral anion guest in the restricted chiral binding space between them (yellow shaded region). The anion is expected to be encapsulated by chiral motifs on both the axle and macrocycle of the rotaxane, allowing them to contribute synergistically to enantio-discrimination.<sup>50</sup> To further appreciate the roles played by the individual axle and macrocycle components for chiral discrimination by a [2]rotaxane, two structurally-similar rotaxane analogues

containing either a chiral macrocycle and achiral axle (Rotaxane **2**), or an achiral macrocycle and chiral axle (Rotaxane **3**) were prepared for comparison. Each chiral rotaxane contains four convergent XB-donor groups positioned around the central interlocked host cavity region of the rotaxane for binding carboxylate/ phosphate motifs of chiral oxoanion guest species. The bulky chiral groups of the guest oxoanions are thus designed to be oriented towards the asymmetric motifs of the three dimensional rotaxane binding cavity to achieve optimal enantioselectivity.

The active metal template (AMT) strategy<sup>51,52</sup> used to synthesise the target chiral XB rotaxanes involved axle formation by copper(I)-catalysed azide-alkyne cycloaddition (CuAAC) reactions through the cavity of a XB macrocycle, by capitalising on the endo/exo-conformational flexibility of the iodotriazole groups for copper(I) *N*-ligation.<sup>53,54</sup> As shown in Scheme 1A, to assemble the macrocycle components (**4.XB** and **5.XB**), direct CuAAC iodotriazole formation from either BINOL- or biphenyl-bis(azide) with an aryl (pro-to)alkyne,<sup>55</sup> followed by deprotection of the methoxymethyl acetal protecting group under acidic conditions afforded the bis-phenol macrocycle precursors. Cyclisation was achieved by reacting equimolar quantities of the bis-phenol precursors with triethylene glycol-bis(tosylate) in the presence of cesium carbonate base to give the target macrocycles. The ability of macrocycle **4.XB** to coordinate copper(I) was established by <sup>1</sup>H NMR titration experiments with [Cu(CH<sub>3</sub>CN)<sub>4</sub>]PF<sub>6</sub> (Section S3.1, Supporting Information).

Thereafter, the neutral XB chiral rotaxanes **6**, **7** and **8** were prepared using 1.0 equivalent of macrocycle (**4.XB** or **5.XB**) and [Cu(CH<sub>3</sub>CN)<sub>4</sub>]PF<sub>6</sub> in the presence of 4.0 and 8.0 equivalents of pyridine-3,5-bis(iodoalkyne) **9** and the appropriate axle azide precursor respectively under an inert nitrogen atmosphere (Scheme 1B). As direct rotaxane formation via two CuAAC reactions in one pot with a bis-alkyne axle precursor is unprecedented, the AMT reaction for preparing rotaxane **6** was monitored by electrospray ionisation mass spectrometry (ESI-MS), which revealed that rotaxane assembly occurred in two steps (Section S3.2, Supporting Information). Initially, a CuAAC reaction between one of the iodoalkyne groups of **9** and the terminal azide axle precursor gave an asymmetrically-substituted pyridine terminal iodoalkyne intermediate, which then reacted with a second azide axle precursor catalysed by **4.XB**-bound copper(I) through the macrocycle cavity to afford the rotaxane product (Scheme 1B). Complete consumption of the axle azide

Chart 1. Structures of the chiral XB [2]rotaxanes and anions investigated.



and iodoalkyne precursors was observed after 3 days, whereupon ESI mass spectrometric analyses of the respective crude rotaxane reaction mixtures showed the presence of rotaxanes **6**, **7** and **8** at  $m/z$  2838, 2582 and 2678  $[M + H]^+$  respectively. Following de-complexation of the copper(I) catalyst with basic aqueous ethylenediamine-tetraacetate (EDTA), the rotaxanes were isolated via chromatographic purification in yields of up to 48%. Interestingly, the chiral (*S*)-serine-derived terminal azide axle precursor afforded slightly higher rotaxane yields (rotaxanes **6** and **8**) compared to its achiral counterpart containing an unfunctionalized propyl spacer (for rotaxane **7**). This may suggest the involvement of secondary non-covalent interactions (e.g. HB) between the azide precursor and the macrocycle which facilitates the threading process necessary for CuAAC-AMT rotaxane formation.

Exclusive mono-methylation of the rotaxanes' axle pyridine moiety was then achieved by reaction of each rotaxane with iodomethane to afford the desired cationic chiral XB [2]rotaxanes, and anion exchange to their hexafluorophosphate salts afforded hosts **1**, **2** and **3**. Notably, the  $^1\text{H}$  NMR spectra of **1** and **3** showed distinct evidence of increased conformational rigidity following methylation of the axle pyridine group. For the neutral rotaxane congeners **6** and **8**, the  $^1\text{H}$  NMR spectra revealed dynamic behavior with the macrocyclic components adopting various conformations around the chiral axle in slow exchange on the NMR timescale. However, axle methylation led to dramatic simplification of the rotaxanes' NMR spectra to give well-defined proton signal environments (see Figure S2-25, Supporting Information). This indicated that the macrocycle components of cationic rotaxanes **1** and **3** were now predominantly locked around the axle, brought about by HB interactions between the axle pyridinium group and the macrocycles' polyether unit. Full synthetic details of all macrocycles, axle precursors and rotaxanes are provided in the Supporting Information, together with unequivocal evidence of the interlocked nature of the cationic rotaxanes **1-3** obtained by two-dimensional  $^1\text{H}$ - $^1\text{H}$  ROESY experiments.

**Chiral Recognition Studies.** The chiral anion discrimination properties of rotaxane **1** was studied using  $^1\text{H}$  NMR titration experiments, where tetrabutylammonium (TBA) salts of chiral anions<sup>56</sup> (Chart 1) were added as separate enantiomers in increasing quantities to individual solutions of the rotaxane in  $d_6$ -acetone/  $\text{D}_2\text{O}$  98:2 ( $v/v$ ). Derivatives of naturally-occurring amino acids were chosen for study due to their biological importance

and accessible enantio-pure forms, as well as chiral BINOL-derived phosphates, which have found important applications in asymmetric catalysis.<sup>57</sup>

Figure 1A shows the perturbations of various proton resonances of rotaxane **1** upon addition of the NBoc-(*S*)-proline carboxylate anion, as a representative example. Downfield shifts were seen for signals arising from the (*S*)-BINOL protons  $H_a$  and  $H_b$  on the macrocycle, as well as proton  $H_3$  on the terphenyl stopper units proximal to the rotaxane binding cavity. Notably, negligible shifts were seen for the inner pyridinium proton ( $H_i$ ) of the axle flanked by iodotriazole groups, suggesting that true to our rotaxane host design, the chiral anion is bound in the space between the macrocyclic and axle components as shown in Chart 1. Importantly, these observations also suggest that the chiral units on the axle and macrocycle are both interacting with the anion bound in the chiral space between them, and hence are both contributing synergistically to chiral discrimination.

In the presence of the opposite guest enantiomer (NBoc-(*R*)-proline carboxylate), significantly different interactions were seen for the proton environments surrounding the rotaxane cavity. Perhaps due to its unique position immediately adjacent to the BINOL moiety on the macrocycle component, the perturbations of the signals arising from the diastereotopic protons  $H_f$  were most sensitive to changes in the conformations and electronic environment of the binding site in the presence of different anion guest enantiomers. For instance, as shown in Figure 1B, the binding isotherm resulting from the shifts of  $H_f$  plotted as a function of anion equivalents achieved saturation more quickly for NBoc-(*S*)-proline carboxylate (black dotted curve) compared to that of the opposite guest enantiomer (red dotted curve). More dramatically, both enantiomers of the BINOL- $\text{PO}_4^-$  anion perturbed the  $H_f$  signals of rotaxane **1** in different directions, with 10.0 molar equivalents of (*S*)-BINOL- $\text{PO}_4^-$  eliciting a significant *upfield* shift of -0.13 ppm and the equivalent amount of (*R*)-BINOL- $\text{PO}_4^-$  giving a much smaller *downfield* shift of only +0.012 ppm. As shown, the highly preorganized and conformationally restricted chiral binding space of rotaxane **1** is capable of effectively discriminating between different guest enantiomers. Non-linear regression analysis of the binding isotherms obtained from monitoring shifts of appropriate proton signals in the rotaxane binding cavity during the titrations (see Figure S4-1, Supporting Information), using the WinEQNMR2 software<sup>58</sup> with a host-guest 1:2 stoichiometric binding model, determined association constants ( $K$ ) as well as the corresponding magnitudes of chiral selectivity ( $\xi = K_S/K_R$ ) for each chiral anion pair

reported in Table 1. Notably, the second association constants ( $K_2$ ) were much smaller in magnitude ( $< 10 \text{ M}^{-1}$ ) compared to the first ( $K_1$ ) for all anion pairs studied, suggesting that one chiral anion guest is predominantly bound within the rotaxane chiral binding cavity, while the second was weakly associated with the bound complex, probably at its periphery. Hence, the values of  $K_1$  were solely used to determine chiral selectivity as only the first anion bound is held within the host cavity and therefore properly influenced by its chiral environment. Amongst the four chiral anion pairs investigated, the most impressive and best enantioselectivities were seen for NBoc-proline carboxylate and BINOL- $\text{PO}_4^-$ , each possessing rigid chiral units. The slightly improved discrimination seen for NBoc-tryptophan carboxylate compared to NBoc-leucine may imply the contribution of steric effects in chiral selectivity.<sup>59,60</sup>

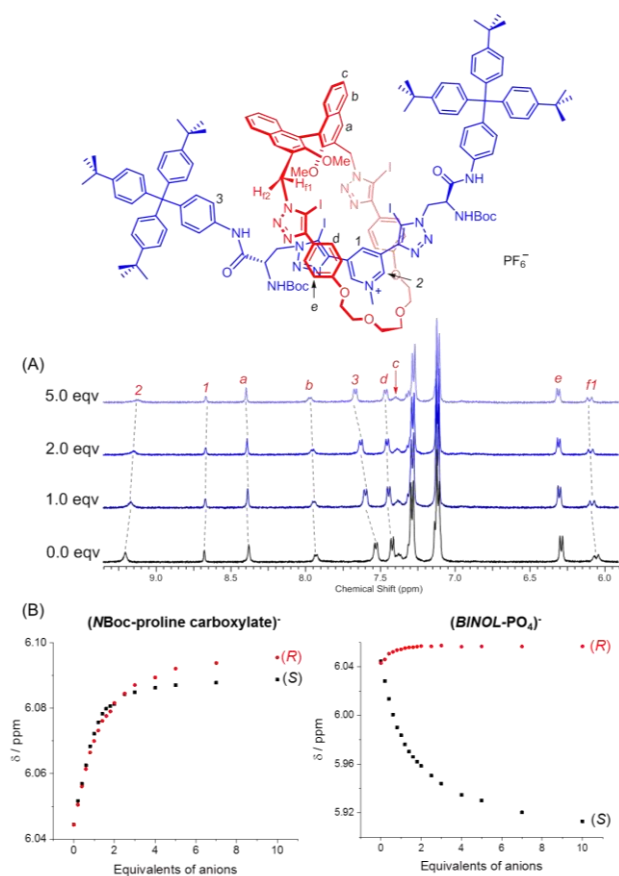


**Figure 1.** (A) Partial  $^1\text{H}$  NMR spectra of rotaxane **1** with 0.0, 1.0, 2.0 and 5.0 equivalents of NBoc-(S)-proline carboxylate; (B) Changes in the chemical shift of proton  $H_{f1}$  with increasing quantities of both enantiomers of NBoc-proline- $\text{COO}^-$  and BINOL- $\text{PO}_4^-$  ([rotaxane **1**] = 1.0 mM,  $d_6$ -acetone/  $\text{D}_2\text{O}$  98:2,  $T = 298 \text{ K}$ ).

To appreciate the importance of the rotaxane's chiral interlocked cavity for enantio-discrimination and the roles played by its XB-donor iodotriazole motifs, analogous  $^1\text{H}$  NMR binding studies were performed using the free axle and macrocycle components as well. For free chiral axle **10** (Figure 2A), the most significant perturbations seen upon NBoc-(S)-proline carboxylate addition were the downfield shifts of the internal pyridinium proton  $H_1$  signals. Although the amide linkages adjacent to the stopper units of the axle are potentially capable of hydrogen bonding with the anion, negligible shifts of the proximal stopper proton  $H_3$  were seen, unlike those of rotaxane **1**, clearly suggesting that the chiral anions were mainly bound by the central pyridinium-3,5-bis(iodotriazole) motif of the free axle. The dominance of the charge-assisted XB interactions for carboxylate binding over competing HB from the amide groups also gives further credence to the proposed anion binding mode of rotaxane **1**, where the oxoanion groups of the chiral guests are mainly held by the iodotriazoles at the core of the rotaxane to orientate their asymmetric portions for interaction with the binding site chiral functionalities (*vide infra*). In addition, from the small shifts of the  $H_4$  and  $H_5$  resonances around the free axle's chiral centres, the anions' binding location appears to limit the stereo-specific host-guest interactions with the bulky asymmetric units responsible for chiral discrimination. Unsurprisingly, WinEQNMR2<sup>58</sup> determination of the association constants of axle **10** with the various chiral anion pairs reveal generally greatly diminished enantioselectivity (Table 1) compared with rotaxane **1**.

$^1\text{H}$  NMR chiral discrimination studies were performed using dicationic macrocycle **11.XB** (synthesis described in Section 1, Supporting Information) instead of its neutral congener **4.XB**, as the latter did not show appreciable binding affinities for any of the chiral anions in  $d_6$ -acetone/  $\text{D}_2\text{O}$  98:2 *v/v*. Titrations of the NBoc-(S)-proline carboxylate oxoanion with free dicationic macrocycle **11.XB** elicited distinct upfield shifts of the macrocycle (S)-BINOL aromatic proton signals  $H_a$ ,  $H_b$ ,  $H_c$  and  $H_d$  (Figure 2B). For comparison, we also synthesized the dicationic (proto)triazolium halogen-free macrocycle analogue **11.HB** (Section 1, Supporting Information) and studied its chiral discrimination properties in the same solvent medium. The addition of NBoc-(S)-proline carboxylate gave negligible shifts of the aromatic BINOL proton resonances on macrocycle **11.HB** despite clear evidence of anion binding which brought about notable perturbations of  $H_f$  and  $H_g$  (Fig. S4-8, Supporting Information). This indicates that the stringent linearity of the XB-carboxylate interactions was instrumental in directing the chiral anion guest for interaction with macrocy-



cle **11.XB**'s (S)-BINOL group for chiral discrimination. This difference is reflected in their respective magnitudes of chiral selectivity for NBoc-proline carboxylate, with **11.XB** ( $K_S/K_R = 0.70 \pm 0.01$ ) proving superior to **11.HB** ( $K_S/K_R = 0.92 \pm 0.05$ ) (see Table S3-1, Supporting Information for enantioselectivity of **11.HB** towards all chiral anion pairs). However from Table 1, the enantioselectivities of **11.XB** still pales in comparison to those of rotaxane **1**, most notably for the conformationally highly-rigid NBoc-proline carboxylate and BINOL- $\text{PO}_4^-$  anion enantiomers. Undoubtedly, this arises from the more complete encapsulation of the chiral anion guest possible with the three-dimensional interlocked binding cavity of rotaxane **1**, allowing a greater number of stereoselective interactions to take place for more effective chiral discrimination (*vide infra*).

After establishing the superiority of rotaxane **1** for chiral anion discrimination compared to its free axle and macrocycle components, we subsequently compared its chiral selectivity with rotaxanes **2** and **3**, possessing one chiral and one achiral component each, via analogous  $^1\text{H}$  NMR titration experiments to determine the importance of each component for chiral discrimination. For both rotaxanes **2** and **3**, the presence of oxoanions caused shifts of the BINOL and biphenyl macrocyclic aromatic protons, respectively, as well as the alkyl proton environments on the axle flanking the anion binding cavity (Figures S4.2 and S4.4, Supporting Information). Owing to the strong charge-assisted XB-interactions arising from the common pyridinium-bis(iodotriazole) motif in the rotaxanes' central region, all anions were bound in the chiral binding space between the macrocycle and axle components likely in a similar manner as rotaxane **1** shown in Chart 1.

A closer inspection of the anion affinities of all XB chiral host systems studied in Table 1 revealed that the general anion binding strengths decreased in the order of axle **10** > rotaxane **1**  $\approx$  rotaxane **3** > macrocycle **11.XB** > rotaxane **2**. Despite having four XB donor groups, the rotaxanes bound the chiral oxoanions surprisingly more weakly than free chiral axle **10** possessing just two iodotriazole units likely due to steric hindrance limiting anion access to the rotaxanes' spatially more restricted binding cavities (*vide infra*). Interestingly, rotaxanes **1** and **3**, which possess HB-donor groups on their axle components (i.e. NHBoc and amide), were able to bind the anions generally more strongly than even dicationic macrocycle **11.XB**, suggesting the important influence of these secondary non-covalent interactions for anion association (*vide infra*). In stark contrast, the absence of these HB motifs on the axle component of rotaxane **2**,

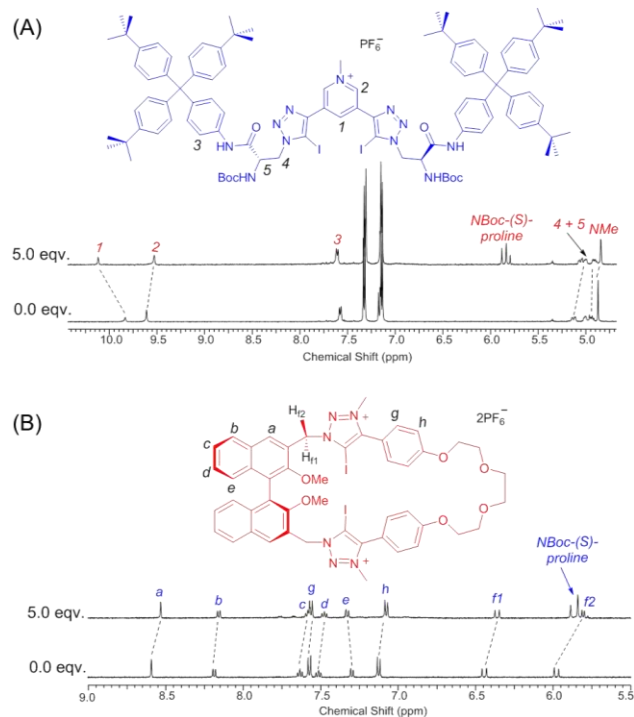


**Figure 2.** Partial  $^1\text{H}$  NMR spectra of (A) free axle **10** and (B) macrocycle **11.XB** with 0.0 and 5.0 equivalents of NBoc-proline- $\text{COO}^-$  ([host] = 1.0 mM,  $d_6$ -acetone/  $\text{D}_2\text{O}$  98:2,  $T = 298$  K).

which contains unfunctionalized achiral propyl spacer units, dramatically reduced its anion binding affinity compared to rotaxanes **1** and **3**, further emphasizing the important roles of these HB motifs for anion binding. In fact, the reduction in anion affinity was so significant that the binding studies of rotaxane **2** had to be performed in a less-competitive solvent mixture of acetone/ $\text{D}_2\text{O}$  99:1 (*v/v*) to achieve appreciable proton shifts for reliable values of association constants to be obtained. However, although all three rotaxanes investigated possess the same structural skeleton, their respective anion binding cavities are very different from one another due to the various combinations of chiral and achiral components. The important consequence of which is that each XB rotaxane host exhibits a unique chiral anion guest preference. For instance, NBoc-(S)-tryptophan carboxylate is bound most strongly by rotaxane **1**, while **2** and **3** bind NBoc-(R)-proline carboxylate with the highest affinity. It is nevertheless noteworthy that the NBoc-proline carboxylate enantiomers exhibit consistently strong anion binding for all chiral XB hosts, with smaller variations in binding affinity compared to the other chiral anion pairs. Likely due to their smaller size compared to all the other anion pairs investigated, they are expected to encounter less steric repulsions with

**Table 1. Anion association constants ( $K/\text{M}^{-1}$ ) for chiral anion pairs and the magnitudes of chiral selectivity ( $\xi$ ) by rotaxanes **1**, **2**, **3**, free axle **10** and macrocycle **11.XB**.<sup>a</sup>**

	$K_S$	$K_R$	$\xi$	$K_S$	$K_R$	$\xi$
	Rotaxane <b>1</b> <sup>b</sup>			Rotaxane <b>2</b> <sup>c</sup>		
(NBoc-Leu) <sup>-</sup>	2450 ± 154	1511 ± 131	1.62 ± 0.17	138 ± 11	471 ± 38	0.29 ± 0.03
(NBoc-Trp) <sup>-</sup>	4990 ± 196	2886 ± 203	1.73 ± 0.14	471 ± 37	760 ± 45	0.62 ± 0.06
(NBoc-Pro) <sup>-</sup>	4298 ± 125	1465 ± 52	2.93 ± 0.13	1719 ± 59	2586 ± 110	0.66 ± 0.04
(BINOL-PO <sub>4</sub> ) <sup>-</sup>	547 ± 16	1170 ± 99	0.47 ± 0.04	354 ± 22	631 ± 48	0.56 ± 0.06
	Rotaxane <b>3</b>			Axle <b>10</b> <sup>d</sup>		
(NBoc-Leu) <sup>-</sup>	$K_1 = 2100 \pm 147$ $K_2 = 62 \pm 5$	$K_1 = 2244 \pm 99$ $K_2 = 49 \pm 3$	$\xi_1 = 0.94 \pm 0.08$	$K_1 = 6027 \pm 321$ $K_2 = 166 \pm 9$	$K_1 = 4630 \pm 86$ $K_2 = 142 \pm 11$	$\xi_1 = 1.30 \pm 0.07$
(NBoc-Trp) <sup>-</sup>	$K_1 = 1905 \pm 107$ $K_2 = 34 \pm 2$	$K_1 = 2253 \pm 138$ $K_2 = 32 \pm 3$	$\xi_1 = 0.85 \pm 0.07$	$K_1 = 2581 \pm 91$ $K_2 = 56 \pm 2$	$K_1 = 1836 \pm 117$ $K_2 = 95 \pm 6$	$\xi_1 = 1.41 \pm 0.10$
(NBoc-Pro) <sup>-</sup>	$K_1 = 4031 \pm 100$ $K_2 = 55 \pm 2$	$K_1 = 4468 \pm 131$ $K_2 = 55 \pm 2$	$\xi_1 = 0.90 \pm 0.03$	$K_1 = 6193 \pm 89$ $K_2 = 33 \pm 1$	$K_1 = 5057 \pm 128$ $K_2 = 39 \pm 1$	$\xi_1 = 1.22 \pm 0.04$
(BINOL-PO <sub>4</sub> ) <sup>-</sup>	$K_1 = 4159 \pm 100$ $K_2 = 86 \pm 3$	$K_1 = 3491 \pm 148$ $K_2 = 93 \pm 4$	$\xi_1 = 1.19 \pm 0.06$	$K_1 = 4861 \pm 122$ $K_2 = 24 \pm 1$	$K_1 = 5942 \pm 270$ $K_2 = 17 \pm 1$	$\xi_1 = 0.82 \pm 0.04$
	Macrocycle <b>11.XB</b> <sup>e</sup>			space left blank		
(NBoc-Leu) <sup>-</sup>	423 ± 3	635 ± 31	0.67 ± 0.03			
(NBoc-Trp) <sup>-</sup>	324 ± 6	488 ± 21	0.66 ± 0.03			
(NBoc-Pro) <sup>-</sup>	3495 ± 64	4961 ± 47	0.70 ± 0.01			
(BINOL-PO <sub>4</sub> ) <sup>-</sup>	854 ± 43	540 ± 24	1.58 ± 0.11			

<sup>a</sup> Values of  $K$  calculated using the WinEQNMR2 software<sup>58</sup> using a host-guest 1:2 binding model in *d*<sub>6</sub>-acetone/ D<sub>2</sub>O 98:2 monitoring the perturbation of proton  $H_{\beta 1}$  for all hosts unless otherwise stated (see Section S4, Supporting Information for more details);  $\xi = K_S/K_R$  only for the first binding event; anions added as TBA salts; [host] = 1.0 mM,  $T = 298\text{ K}$ . <sup>b</sup> Although rotaxane **1** bound chiral anions with host-guest 1:2 binding stoichiometry,  $K_2 < 10\text{ M}^{-1}$  for all cases. Axle proton  $H_2$  monitored for both enantiomers of (BINOL-PO<sub>4</sub>)<sup>-</sup> due to small shifts of  $H_{\beta 1}$  seen for the (*R*)-guest. <sup>c</sup> Titrations were performed in *d*<sub>6</sub>-acetone/ D<sub>2</sub>O 99:1 due to weak binding. With the exception of (BINOL-PO<sub>4</sub>)<sup>-</sup> for which  $H_{\beta 1}$  gave substantial shifts, axle pyridinium proton  $H_1$  was monitored instead; values of  $K$  fit using a host-guest 1:1 binding model, with no evidence of a second binding event occurring. <sup>d</sup> Internal pyridinium proton  $H_1$  monitored. <sup>e</sup>  $H_{\beta 1}$  monitored,  $K_2 < 10\text{ M}^{-1}$ .

the bulky chiral groups decorating the hosts' binding cavities, allowing deeper penetration and hence stronger binding.

Figure 3 summarizes the guest enantiomer preference and magnitudes of enantioselectivity by all chiral XB host molecules from Table 1 visually, which reveals further insights regarding the chiral discrimination behavior of the rotaxanes. Regarding the magnitudes of chiral selectivity, given that only one rotaxane component surrounding the anion binding site is chiral in rotaxanes **2** and **3**, fewer enantio-specific host-guest interactions with the bound chiral anion can be expected compared to rotaxane **1**, resulting in generally poorer enantioselectivity. Interestingly, replacing the chiral axle of rotaxane **1** with an achiral axle in **2** generally afforded

only small reductions in selectivity, with NBoc-leucine carboxylate being a notable exception. However, substituting the chiral macrocycle component in rotaxane **1** for an achiral counterpart in rotaxane **3** resulted in expectedly poor discrimination between both enantiomers for all chiral anion pairs investigated. In fact, the general enantioselectivity for rotaxane **3** was found to be even poorer than that of axle **10**, with the bulky and rigid BINOL-PO<sub>4</sub><sup>-</sup> enantiomers being most effectively discriminated with a modest preference of only  $1.19 \pm 0.06$  for the (*S*)-enantiomer. This suggests that the macrocycle components of our XB rotaxane design exert dominating influences on their effectiveness in chiral discrimination, which may be partly due to the greater rigidity and larger steric bulk of the macrocycle's chiral (*S*)-BINOL group

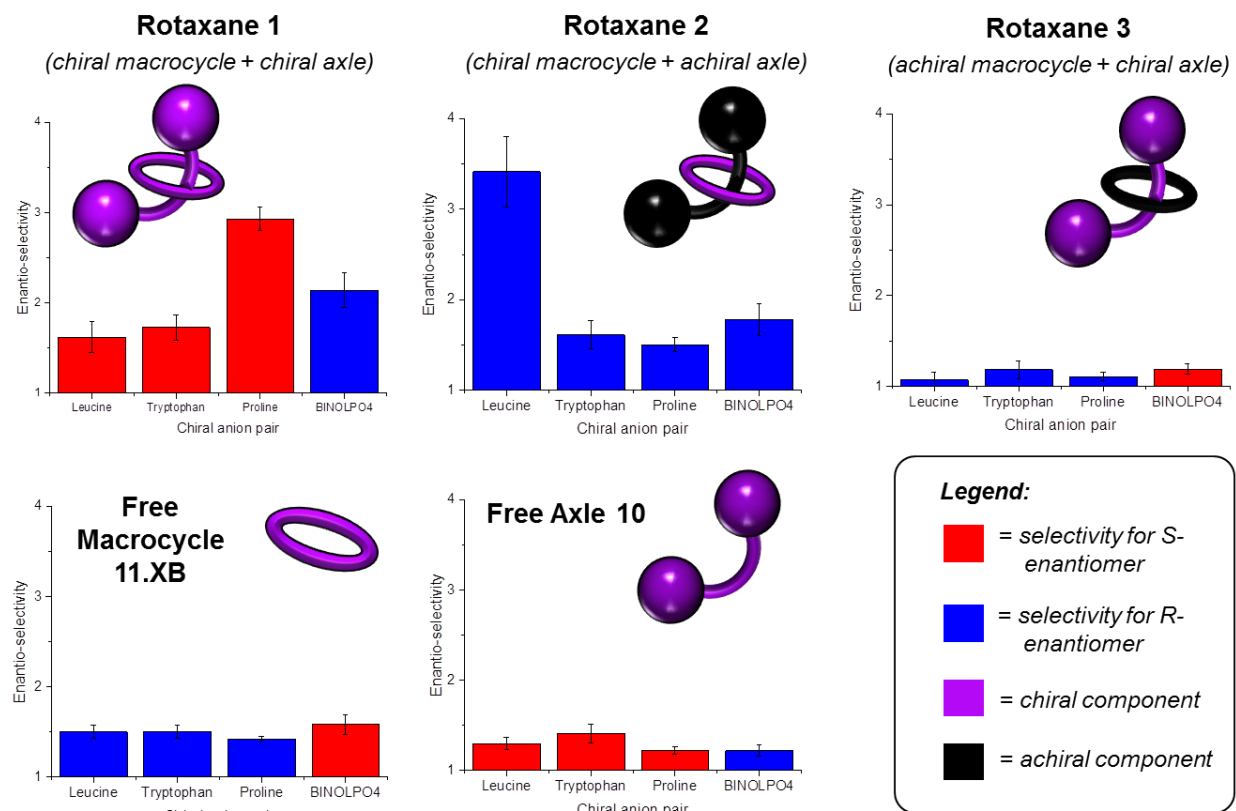


**Figure 3.** Bar charts summarizing the enantiomer binding preference and magnitudes of chiral selectivity aspects of chiral discrimination by rotaxanes **1**, **2** and **3**, as well as those for their chiral non-interlocked macrocycle and axle components. All amino acid derivatives used are *N*Boc-protected.

as compared to the point-chiral (*S*)-serine- derived asymmetric units of the axle.<sup>61</sup>

While the macrocycle component appears to dominate the magnitude of chiral selectivity, its influences on the rotaxanes' enantiomer binding preferences are less obvious. For instance, although it appears that the macrocycle component of rotaxane **2**, being the only chiral component, is driving a generally similar preference for binding the (*R*)-anion enantiomers as the free macrocycle **11.XB**, the selectivity patterns observed are not entirely identical, as exemplified with BINOL-PO<sub>4</sub><sup>-</sup>. Rotaxane **3**, bearing only the chiral axle, surprisingly exhibits the opposite enantiomer binding preference to that of the chiral axle **10**. Although these two examples seem to suggest that the influence of the macrocycle outweighs that of the axle in enantiomer binding preference as well, rotaxane **1** displays the same preference as chiral axle **10**, contrary to the expected macrocycle-dominated behavior. As previously noted, the structural uniqueness of

each chiral rotaxane anion binding cavity gives rise to different contributions of attractive and repulsive non-covalent interactions to anion binding. Hence, it is the interplay of these multiple interactions that result in subtle energy differences between the various rotaxane-anion diastereomeric complexes, which govern enantiomer preference in each case, making it difficult to predict their behavior by extrapolation from the free chiral axle and macrocycle host molecules alone. Nevertheless, all point-chiral amino acid derivatives were found to exhibit the same chiral selectivity pattern with the host molecules (e.g. all (*S*)-selective for rotaxane **1**). However interestingly, the chiral BINOL-PO<sub>4</sub><sup>-</sup> enantiomers generally exhibited the opposite selectivities as the amino acid derivatives (*vide infra*).

**Molecular Modeling Studies.** MD simulations performed in solution offered further insights on the chiral recognition behavior of rotaxanes **1-3**, axle **10** and mac-



rocycle **11.XB**. As the enantio-discrimination of the *N*Boc-proline carboxylate enantiomers is largely representative of the various amino acid-derived chiral guests studied (Figure 3), both enantiomers were used as the model guest species for this theoretical investigation. The initial host-guest binding scenarios were generated in the gas-phase via geometry optimizations with the CAM-B3LYP functional using TeraChem,<sup>62–67</sup> before being investigated in solution with MD simulations performed using the AMBER16 software.<sup>68–70</sup> The quantum mechanics and classical force field calculations were performed taking advantage of GPU acceleration in both application suites.

During the initial DFT geometry optimizations, two starting binding scenarios were generated for each *N*Boc-proline carboxylate guest enantiomer in each host’s binding site (called  $S_A$ ,  $S_B$ ,  $R_A$  and  $R_B$ ), differing in the orientation of the anion’s chiral pyrrolidine ring, as detailed in Section S5 of the Supporting Information. Due to the size of rotaxanes **1-3**, the stopper groups of their axle components were initially capped with *tert*-butyl groups, affording the corresponding pseudo-rotaxanes. The *N*Boc-proline enantiomers were then positioned in each rotaxane’s chiral interlocked binding pocket, held by at least two putative XB interactions. Using these DFT-optimized host-guest complexes (Figures S5-1 to S5-3, Supporting Information), the entire rotaxane host structures were then restored by re-attaching the bulky stopper units for the subsequent MD simulations. Thereafter, each initial host-guest complex was immersed in periodic cubic boxes composed of suitable number of water and acetone molecules in accordance with the <sup>1</sup>H NMR titrations (Table 1). The rotaxanes’ components were described with the General AMBER Force Field (GAFF)<sup>71,72</sup> and the XB interactions were modelled using the extra point of charge approach.<sup>73</sup> The remaining force field parameters and simulation details are provided in Section S5.3, Supporting Information. Five independent 20 ns MD runs were performed for each initial binding arrangement, and the subsequent analyses of the MD production data is based on the most frequent binding arrangements obtained by cluster analysis of the concatenated trajectory files as detailed in Section S5.3, Supporting Information.

Rotaxane **1** exhibits distinct binding scenarios with each enantiomer of *N*Boc-proline carboxylate. With *N*Boc-(*S*)-proline two main binding arrangements were obtained independently of the initial scenarios  $S_A$  or  $S_B$ . The anion is held within rotaxane **1**’s chiral binding pocket in the space between the axle and macrocycle components throughout all simulation runs, bound by

XB and HB interactions from both interlocked components. Notably, several water molecules bound to the host by XB and HB interactions were found to actively participate in anion binding by forming bridging HB interactions with the carboxylate anion held in the rotaxane’s binding cavity (see Table S5-1, Supporting Information). For instance, in the most frequent binding structure (Figure 4A), one oxygen atom of the anion’s carboxylate group participates in direct XB interaction with the axle’s central pyridinium-3,5-bis(iodotriazole) motif, while the other forms a HB network with water molecules held together by a XB interaction with the macrocycle iodotriazole unit ( $C-I\cdots OH_2$ ), as well as by the *N*Boc and amide units on the axle. In the second most common binding arrangement (Figure 4B), the anion’s carboxylate group is held by two direct XB interactions from each iodotriazole on the macrocycle component, and one from the axle. The spatial disposition of the anion brings it near the chiral units flanking the binding site, resulting in the signal perturbations from the rotaxane’s axle and macrocycle components seen during the <sup>1</sup>H NMR titrations (Figure 1).

Owing to the spatial and geometric constraints of rotaxane **1**’s chiral binding cavity, MD simulations revealed a generally less favorable association with *N*Boc-(*R*)-proline carboxylate. Simulations starting from the  $R_B$  initial binding scenario (Section S5, Supporting Information) resulted in systematic decomplexation of the anion along the five MD independent runs. Slightly more preferential binding was observed for the  $R_A$  starting scenario, with the most frequent binding arrangement (Figure 4C) showing one weak and sporadically-broken direct halogen bond from the rotaxane’s macrocycle component, which is assisted by a  $(N-H)_{\text{host}}\cdots OH_2\cdots (O=C)_{\text{guest}}$  bridge from the rotaxane axle’s *N*Boc unit (average dimensions and frequencies of the XB interactions are collected in Tables S5-2 and S5-3 in the Supporting Information for the anions and water molecules respectively). However, for a significant period of sampling, the anion was also found outside the rotaxane binding pocket, interacting peripherally only with the axle’s amide NH group. This dynamical behavior suggests a significantly weaker interaction between rotaxane **1** and the *N*Boc-(*R*)-proline carboxylate than with the (*S*)-enantiomer, as illustrated in Fig. S5-4 (Supporting Information), where the ratio of the host-guest XB interaction frequency are plotted for both anion enantiomers. These structural findings stress the importance of the XB interactions on the anion enantioselective recognition of **1**, corroborating the binding preferences determined by <sup>1</sup>H NMR titrations.

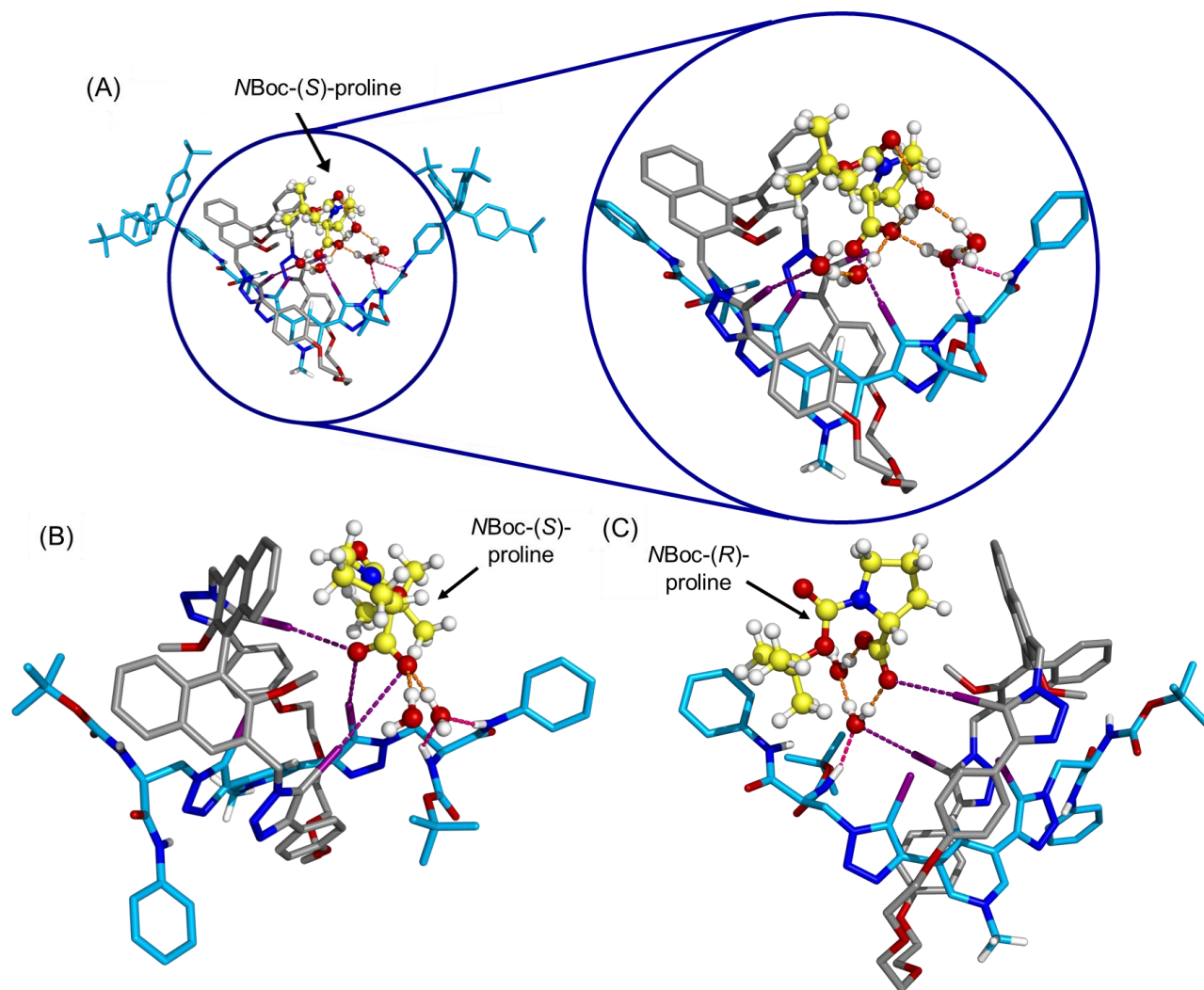


**Figure 4.** (A) The most common binding arrangement of rotaxane **1** with NBoc-(*S*)-proline carboxylate, with the binding cavity expanded; (B) View of the second most common arrangement of NBoc-(*S*)-proline carboxylate within the rotaxane binding cavity; (C) Most common binding arrangement of rotaxane **1** with the (*R*)-enantiomer. The XB interactions from the iodine atoms are indicated by purple dashes, while HB interactions between water molecules are shown in orange and between water molecules and the axle amide binding sites in pink. The stopper groups are not shown in (B) and (C) for clarity.

The modeling studies also provided clear insights on the observed superiority of rotaxane **1** for chiral recognition compared with free axle **10** and macrocycle **11.XB**. From the two initial DFT-optimised binding scenarios for each anion enantiomer with macrocycle **11.XB** ( $S_A$ ,  $S_B$ ,  $R_A$  and  $R_B$ ), and the single binding arrangement for each enantiomer with axle **10** (Figures S5-5 and S5-6 in the Supporting Information), MD simulations were performed using the same approach as rotaxanes **1-3** resulting in the representative anion binding complex structures shown in Figure 5. For axle **10**, the lack of sterics conferred by the macrocycle unit of rotaxane **1** allows

both hydrated NBoc-proline carboxylate guest enantiomers to be tightly bound to the axle's central pyridinium-3,5-bis(iodotriazole) motif via direct XB interactions (Figure 5A), consistent with the signal perturbations seen during the  $^1\text{H}$  NMR titrations in Figure 2A, and accounts for its strong anion affinities (Table 1). Consequently, both anion enantiomers are able to interact only indirectly with the axle's point-chiral amide binding units through water bridges, which is in particular evident with NBoc-(*R*)-proline carboxylate, justifying the axle's general poor enantioselectivity. Furthermore, the

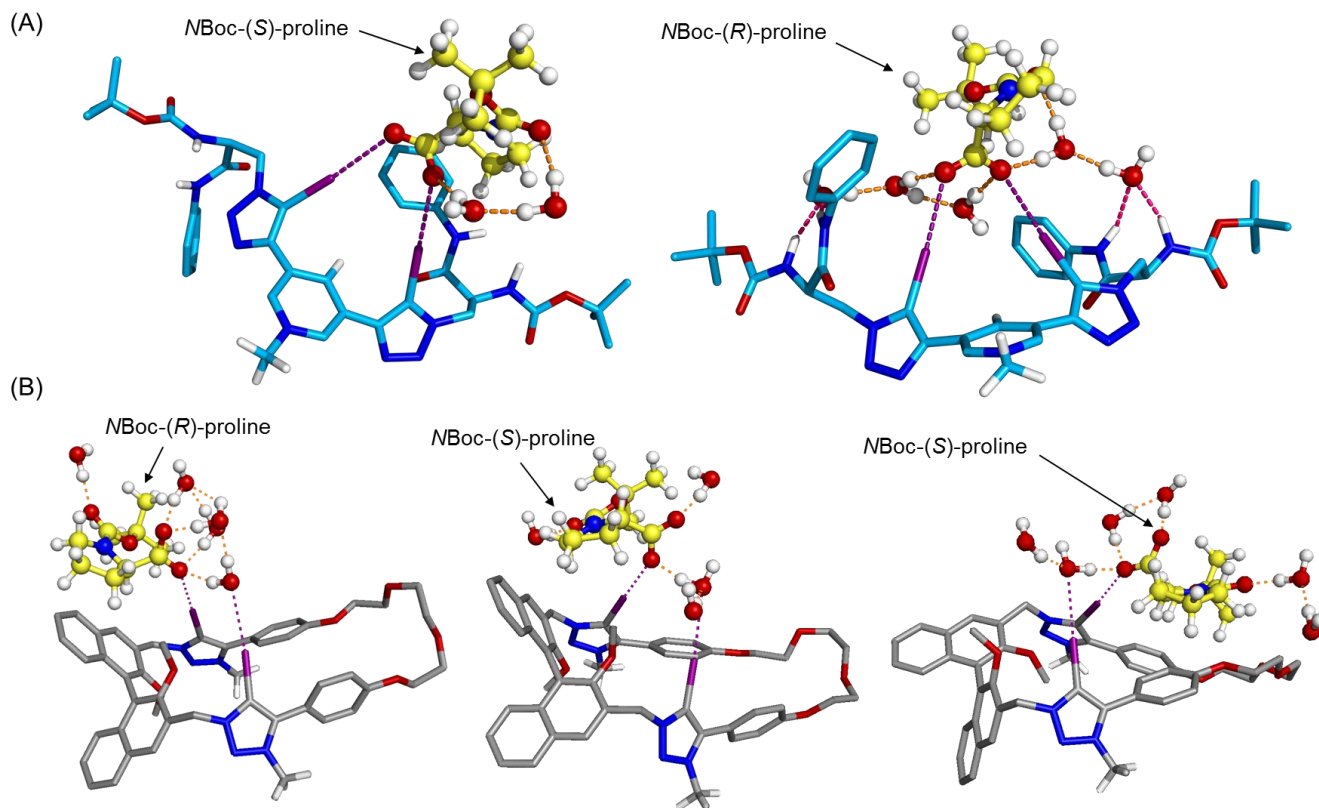


**Figure 5.** (A) Illustrative binding scenarios of axle **10** (stoppers removed for clarity) with NBoc-(S)-proline (left) and NBoc-(R)-proline (right); (B) Most frequent binding scenarios of free macrocycle **11.XB** with NBoc-(R)-proline carboxylate (left) and the opposite enantiomer (middle and right respectively). XB and HB interactions are depicted as dashed lines as described in Figure 4.

XB interactions to NBoc-(S)-proline carboxylate are maintained throughout the sampling time, while those to the (R)-guest enantiomer are sporadically interrupted, with one halogen bond being occasionally established with water molecules (Tables S5-4 and S5-5 in the Supporting Information). This manifests in the observed modest chiral selectivity for NBoc-(S)-proline carboxylate.

In all binding arrangements of NBoc-(S/R)-proline carboxylate anions with free macrocycle **11.XB**, the anions are invariably held a considerable distance above the plane of the macrocycle by highly linear XB interactions (see Table S5-4, Supporting Information). As shown in Figure 5B (left and middle), the most common binding conformations adopted by both (R)- and (S)-anion enantiomers along the 200 ns simulation time involves their rigid pyrrolidine rings held close to the chiral (S)-BINOL motif on the macrocycle, differing slightly in their relative spatial separation and orientations. Each anion enantiomer is bound via only one carboxylate oxygen atom, comprising a direct XB interaction to an iodotri-

azolium group and an indirect association to the second iodotriazolium bridged by a water molecule (Table S5-5, Supporting Information). Notably, this XB coordination arrangement also allows the anion to adopt a binding conformation oriented far away from the macrocycle (S)-BINOL unit. For instance, the second most common binding arrangement of NBoc-(S)-proline carboxylate involves the entire anion being held above the achiral portions of **11.XB** (Figure 5B, right). Compared to the restricted binding cavity of rotaxane **1**, which forces both anion enantiomers to adopt very different binding arrangements, the poorly preorganized binding space of macrocycle **11.XB** allows the guest enantiomers to adopt a greater range of spatially and geometrically more flexible binding conformations. As a consequence, opposite enantiomers can display very similar binding arrangements resulting in the much poorer chiral discrimination of **11.XB** compared with rotaxane **1** (see Table 1).

Analogous MD simulations on the binding of NBoc-(S/R)-proline carboxylate enantiomers to rotaxanes **2** and **3** also shed light on their chiral discrimination behavior.

With rotaxane **2**, bearing only a chiral macrocycle subunit, MD runs revealed that the (*R*)-carboxylate is more strongly bonded to the rotaxane binding cavity compared to the (*S*)-enantiomer, accounting for the rotaxane's observed (*R*)-selectivity. In the most common binding scenario shown in Figure 6A (generated from the  $R_B$  initial binding arrangement), the anion is bound by three synergetic direct XB interactions between its carboxylate unit and the iodotriazoles in the rotaxane binding site (see Table S5-2, Supporting Information). Even in the presence of reduced water content (acetone/ water 99:1 *v/v*), these XB interactions are susceptible to bridging by water molecules to form  $(C-I)_{\text{host}} \cdots (OH_2)_2 \cdots (O=C)_{\text{anion}}$  networks, as depicted in Fig. S5-7, Supporting Information. On the other hand, simulations starting from the  $R_A$ ,  $S_A$  and  $S_B$  optimized structures (Fig S5-2, Supporting Information) result in the fully hydrated anions systematically leaving rotaxane **2**'s binding pocket during the first 10 ns of sampling time in the five MD runs. Notably, replacing the chiral (*S*)-serine derived axle of rotaxane **1** with the propyl spacer in rotaxane **2** prevents the formation of  $(N-H)_{\text{host}} \cdots OH_2 \cdots (O=C)_{\text{anion}}$  bridges, which aid in anchoring the anion within the rotaxane's cavity (shown in Figure 4A). This loss translates to dramatically reduced anion binding strength.

Replacing the bulky chiral (*S*)-BINOL group on rotaxane **1**'s macrocycle component with the achiral biphenyl spacer in rotaxane **3** considerably enlarges the conformational possibilities for anion binding within the rotaxane cavity. Consequently, the obtained MD binding scenarios (Fig. S5-8, Supporting Information) of the host-guest diastereomeric complexes were found to be highly dependent on the initial DFT-optimized binding arrangements (Fig S5-3, Supporting Information). The most frequent binding conformations with NBoc-(*S*)-proline carboxylate involve only two XB interactions, with some HB assistance between the axle component and the NBoc group of the anion (Figure 6B, top). Contrastingly, the (*R*)-guest is typically held by three XB interactions, comprising of two from the macrocycle component and one from the axle (see Figure 6B bottom and Table S5-2, Supporting Information). Furthermore, these XB binding interactions are often assisted by water-bridged hydrogen bonds similar to rotaxane **1**, accounting for the appreciable and comparable anion affinities exhibited by rotaxane **3** (Table 1). Generally, the more frequent XB interactions observed for the NBoc-(*R*)-proline carboxylate likely accounts for its selectivity over the (*S*)-enantiomer. Nonetheless, it is noteworthy that the preferential carboxylate binding by the XB donors in the central portion of the rotaxane directs the

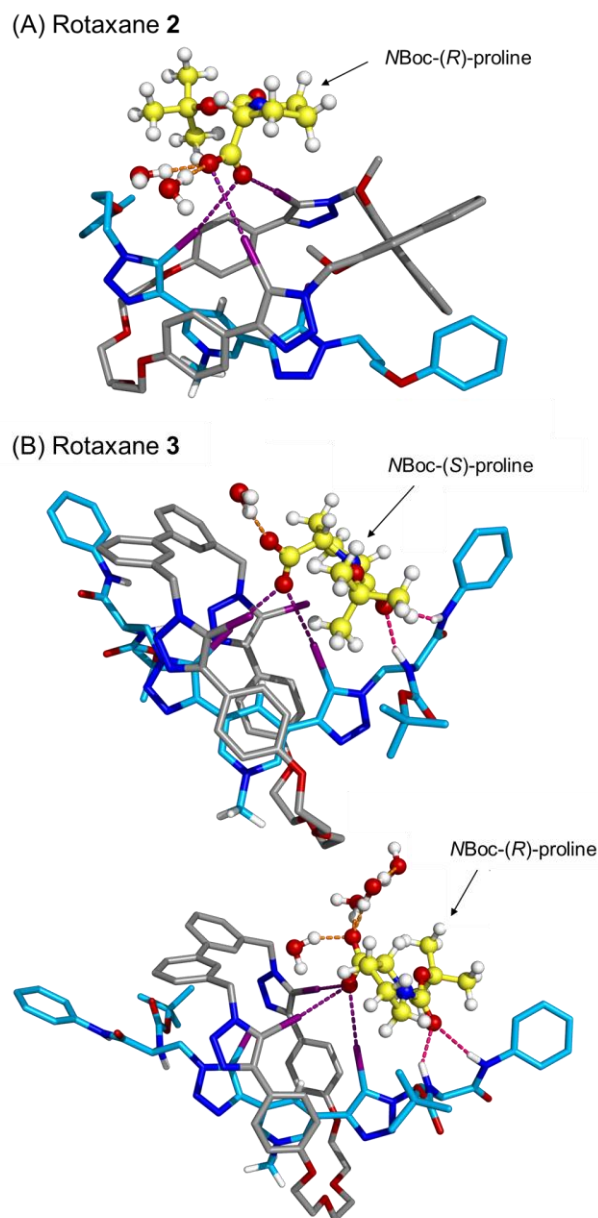


**Figure 6.** (A) Illustrative binding scenario of rotaxane **2** with NBoc-(*R*)-proline; (B) Expanded views of the most frequent binding arrangements of NBoc-(*S/R*)-proline carboxylate with rotaxane **3** (see Fig S5-8, Supporting Information for full views of all binding scenarios). All stoppers were omitted for clarity. XB and HB interactions are depicted as dashed lines as described in Figure 4.

orientation of anion coordination in each binding pocket. Due to the geometric flexibility of anion binding in rotaxane **3**'s binding pocket, the proline's chiral pyrrolidine ring can be either oriented towards the achiral biphenyl spacer on the macrocycle component (Figure S5-8, Supporting Information), or held above the axle's point chiral-unit by poorly-directional HB interactions



showing significant deviations from linearity, bridged by water molecules in some cases. These factors, coupled with the axle's conformationally-flexible point-chiral groups, allows opposite anion enantiomers to adopt remarkably similar binding arrangements (Figure 6B). Contrastingly for rotaxanes **1** and **2**, the XB-directed anion binding geometries forces the prolines' asymmetric units into close proximity with the macrocycle components' rigid and sterically-bulky chiral (*S*)-BINOL groups (Figures 4 and 6A). This likely accounts for the observed dominance of the chiral macrocycle in the rotaxane structure for effective chiral discrimination to occur (Figure 3).

Finally, our modeling experiments also yielded valuable insights on the general opposite enantiomer preference observed for BINOL-PO<sub>4</sub><sup>-</sup> compared to the amino acid anion derivatives. Using rotaxane **1**, MD simulations based on the DFT optimized structures of the best-fit single binding arrangement of (*S/R*)-BINOL-PO<sub>4</sub><sup>-</sup> in the rotaxane binding cavity (see Figure S5-9, Supporting Information) were carried out, which confirmed the stability of both host-guest diastereomeric complexes along the five independent 20 ns MD runs. Each anion enantiomer is bound, via a single oxygen atom, by two convergent XB interactions of comparable dimensions exclusively from the rotaxane axle component's iodotriazoles (Figure S5-10, Supporting Information). Moreover, the (*R*)-BINOL-PO<sub>4</sub><sup>-</sup> is further stabilized by favorable  $\pi\cdots\pi$  stacking interactions with the helicoidal (*S*)-BINOL unit on the macrocycle (shown in Figure S5-10 bottom, Supporting Information). Contrastingly, the relative spatial disposition of the aromatic rings of the (*S*)-BINOL-PO<sub>4</sub><sup>-</sup> guest does not favor the formation of these interactions (Figure S5-10 top, Supporting Information), accounting for the observed preference for (*R*)-BINOL-PO<sub>4</sub><sup>-</sup>.

## CONCLUSIONS

In summary, we have synthesized a family of novel XB chiral [2]rotaxanes using an active metal template approach, and studied their enantioselective anion recognition properties. The presence of a chiral macrocycle component in the rotaxane host design was found to be essential for enantioselective anion binding due to the chiral anion guest orientations dictated by XB interactions, allowing generally superior chiral discrimination properties compared to the free axle and macrocycle components. Contrastingly, the presence of a chiral axle exerted relatively minor influence on the rotaxanes' chiral selectivity as a whole. Notably, the various combinations of chiral and achiral macrocycle and axle compo-

nents led to each rotaxane having unique enantiomer binding preferences, which could not be easily predicted *a priori*. Through MD simulations, the chiral selectivities of each rotaxane were shown to arise from a complex and subtle interplay of attractive and repulsive non-covalent interactions occurring between the chiral guest anions and the rotaxanes' chiral binding cavities in three dimensions, akin to natural enzymes.<sup>74-76</sup> These *in silico* studies also revealed the unexpected influence of the hydration shell of each chiral oxoanion towards their binding affinities and chiral selectivities. Representing the first detailed study of the use of chiral [2]rotaxanes for anion enantio-discrimination, our present findings provide important insights on how this emerging class of molecules function as chiral selectors, which will stimulate further exploitations in catalysis,<sup>30,77-80</sup> drug delivery<sup>81</sup> and nanotechnological<sup>82-84</sup> applications.

## ASSOCIATED CONTENT

### Supporting Information

Detailed synthetic procedures for all novel compounds, characterization data, binding isotherms for chiral anions, additional structures and details from molecular modeling are provided. The Supporting Information is available free of charge on the ACS Publications website.

## AUTHOR INFORMATION

### Corresponding Author

\* paul.beer@chem.ox.ac.uk

### Author Contributions

The manuscript was written through contributions of all authors. / All authors have given approval to the final version of the manuscript.

## ACKNOWLEDGMENT

J.Y.C.L thanks the Agency for Science, Technology and Research (A\*STAR), Singapore, for postgraduate funding. The theoretical studies were supported by project P2020-PTDC/QEQ-SUP/4283/2014 as well as by CICECO – Aveiro Institute of Materials (UID/CTM/50011/2013) and iBiMED – Institute of Biomedicine (UID/BIM/04501/2013), financed by National Funds through the FCT/MEC and, when applicable, co-financed by FEDER through COMPETE, under the PT2020 Partnership Agreement. I.M. thanks the FCT for the PhD scholarship SFRH/BD/87520/2012.

## REFERENCES

- (1) Jo, H. H.; Lin, C.-Y.; Anslyn, E. V. *Acc. Chem. Res.* **2014**, 47 (7), 2212–2221.

- (2) Finn, M. G. *Chirality* **2002**, *14* (7), 534–540.
- (3) Hembury, G. A.; Borovkov, V. V.; Inoue, Y. *Chem. Rev.* **2008**, *108* (1), 1–73.
- (4) Izake, E. L. *J. Pharm. Sci.* **2007**, *96* (7), 1659–1676.
- (5) Phipps, R. J.; Hamilton, G. L.; Toste, F. D. *Nat Chem* **2012**, *4* (8), 603–614.
- (6) Brak, K.; Jacobsen, E. N. *Angew. Chem. Int. Ed.* **2013**, *52* (2), 534–561.
- (7) Mahlau, M.; List, B. *Angew. Chem. Int. Ed.* **2013**, *52* (2), 518–533.
- (8) Bauer, E. B. *Chem Soc Rev* **2012**, *41* (8), 3153–3167.
- (9) Christmann, M.; Brase, S. *Asymmetric Synthesis*; Wiley-VCH: Weinheim: Germany, 2008.
- (10) Mezzetti, A.; Schrag, J. D.; Cheong, C. S.; Kazlauskas, R. J. *Chem. Biol.* **2005**, *12* (4), 427–437.
- (11) Ema, T.; Okuda, K.; Watanabe, S.; Yamasaki, T.; Minami, T.; Esipenko, N. A.; Anzenbacher, P. *Org. Lett.* **2014**, *16* (5), 1302–1305.
- (12) Rossi, S.; Kyne, G. M.; Turner, D. L.; Wells, N. J.; Kilburn, J. D. *Angew. Chem. Int. Ed.* **2002**, *41* (22), 4233–4236.
- (13) Sessler, J. L.; Andrievsky, A.; Král, V.; Lynch, V. J. *Am. Chem. Soc.* **1997**, *119* (40), 9385–9392.
- (14) Li, Z.-B.; Lin, J.; Pu, L. *Angew. Chem.* **2005**, *117* (11), 1718–1721.
- (15) Sansone, F.; Baldini, L.; Casnati, A.; Lazzarotto, M.; Uguzzoli, F.; Ungaro, R. *Proc. Natl. Acad. Sci.* **2002**, *99* (8), 4842–4847.
- (16) Miyaji, H.; Hong, S.-J.; Jeong, S.-D.; Yoon, D.-W.; Na, H.-K.; Hong, J.; Ham, S.; Sessler, J. L.; Lee, C.-H. *Angew. Chem. Int. Ed.* **2007**, *46* (14), 2508–2511.
- (17) Langton, M. J.; Beer, P. D. *Acc. Chem. Res.* **2014**, *47* (7), 1935–1949.
- (18) Knighton, R. C.; Beer, P. D. *Chem Commun* **2014**, *50* (13), 1540–1542.
- (19) Romero, J. R.; Aragay, G.; Ballester, P. *Chem Sci* **2017**, *8* (1), 491–498.
- (20) Caballero, A.; Zapata, F.; Beer, P. D. *Coord. Chem. Rev.* **2013**, *257* (17–18), 2434–2455.
- (21) Brown, A.; Beer, P. D. *Chem Commun* **2016**, *52* (56), 8645–8658.
- (22) Lim, J. Y. C.; Marques, I.; Thompson, A. L.; Christensen, K. E.; Félix, V.; Beer, P. D. *J. Am. Chem. Soc.* **2017**, *139* (8), 3122–3133.
- (23) Neal, E. A.; Goldup, S. M. *Chem Commun* **2014**, *50* (40), 5128–5142.
- (24) Ogoshi, T.; Yamafuji, D.; Aoki, T.; Kitajima, K.; Yamagishi, T.; Hayashi, Y.; Kawauchi, S. *Chem. – Eur. J.* **2012**, *18* (24), 7493–7500.
- (25) Shinoda, S.; Maeda, T.; Miyake, H.; Tsukube, H. *Supramol. Chem.* **2011**, *23* (3–4), 244–248.
- (26) Mohry, A.; Vögtle, F.; Nieger, M.; Hupfer, H. *Chirality* **2000**, *12* (2), 76–83.
- (27) Reuter, C.; Mohry, A.; Sobanski, A.; Vögtle, F. *Chem. – Eur. J.* **2000**, *6* (9), 1674–1682.
- (28) Schmidt, T.; Schmieder, R.; Müller, W. M.; Kiupel, B.; Vögtle, F. *Eur. J. Org. Chem.* **1998**, *1998* (9), 2003–2007.
- (29) J. Cantrill, S.; C. T. Fyfe, M.; M. Heiss, A.; Fraser Stoddart, J.; J. P. White, A.; J. Williams, D. *Chem Commun* **1999**, No. 13, 1251–1252.
- (30) Cakmak, Y.; Erbas-Cakmak, S.; Leigh, D. A. *J. Am. Chem. Soc.* **2016**, *138* (6), 1749–1751.
- (31) Mitchell, D. K.; Sauvage, J.-P. *Angew. Chem. Int. Ed. Engl.* **1988**, *27* (7), 930–931.
- (32) Perret-Aebi, L.-E.; von Zelewsky, A.; Dietrich-Buchecker, C.; Sauvage, J.-P. *Angew. Chem.* **2004**, *116* (34), 4582–4585.
- (33) Bordoli, R. J.; Goldup, S. M. *J. Am. Chem. Soc.* **2014**, *136* (13), 4817–4820.
- (34) Mitra, R.; Thiele, M.; Octa-Smolín, F.; Letzel, M. C.; Niemeyer, J. *Chem Commun* **2016**, *52* (35), 5977–5980.
- (35) Glen, P. E.; O'Neill, J. A. T.; Lee, A.-L. *Tetrahedron* **2013**, *69* (1), 57–68.
- (36) Hiratani, K.; Kaneyama, M.; Nagawa, Y.; Koyama, E.; Kanesato, M. *J. Am. Chem. Soc.* **2004**, *126* (42), 13568–13569.
- (37) Cavallo, G.; Metrangolo, P.; Milani, R.; Pilati, T.; Priimagi, A.; Resnati, G.; Terraneo, G. *Chem. Rev.* **2016**, *116* (4), 2478–2601.
- (38) Beale, T. M.; Chudzinski, M. G.; Sarwar, M. G.; Taylor, M. S. *Chem Soc Rev* **2013**, *42* (4), 1667–1680.
- (39) Gilday, L. C.; Robinson, S. W.; Barendt, T. A.; Langton, M. J.; Mullaney, B. R.; Beer, P. D. *Chem. Rev.* **2015**, *115* (15), 7118–7195.
- (40) Kaasik, M.; Kaabel, S.; Kriis, K.; Järving, I.; Aav, R.; Rissanen, K.; Kanger, T. *Chem. – Eur. J.* **2017**, *23* (30), 7337–7344.
- (41) Peluso, P.; Mamane, V.; Aubert, E.; Dessì, A.; Dallochio, R.; Dore, A.; Pale, P.; Cossu, S. *Enantioseparations* **2016**, *1467*, 228–238.
- (42) Lim, J. Y. C.; Marques, I.; Ferreira, L.; Felix, V.; Beer, P. D. *Chem Commun* **2016**, *52* (32), 5527–5530.
- (43) Borissov, A.; Lim, J. Y. C.; Brown, A.; Christensen, K. E.; Thompson, A. L.; Smith, M. D.; Beer, P. D. *Chem Commun* **2017**, *53* (16), 2483–2486.
- (44) Kubik and co-workers have very recently reported the synthesis of a chiral XB pseudopeptide based macrocycle which binds halides in 2.5% water/DMSO: Mungalpara, D.; Stegmüller, S.; Kubik, S. *Chem Commun* **2017**, *53* (37), 5095–5098.
- (45) Pu, L. *Acc. Chem. Res.* **2012**, *45* (2), 150–163.
- (46) The macrocycle and axle components of rotaxanes **1-3** are designed to be symmetric (i.e. identical groups on both sides of a mirror plane passing through the center of each component) to prevent the rotaxanes from exhibiting additional mechanically bonded chirality.
- (47) Wisner, J. A.; Beer, P. D.; Drew, M. G. B. *Angew. Chem. Int. Ed.* **2001**, *40* (19), 3606–3609.
- (48) Wisner, J. A.; Beer, P. D.; Drew, M. G. B.; Sambrook, M. R. *J. Am. Chem. Soc.* **2002**, *124* (42), 12469–12476.
- (49) White, N. G.; Serpell, C. J.; Beer, P. D. *Cryst. Growth Des.* **2014**, *14* (7), 3472–3479.
- (50) Despite the symmetry of the axle component, only one guest anion is expected to be predominantly bound in the rotaxane cavity due to the spatial constraints of the binding site and size of respective chiral anion guest species.
- (51) Aucagne, V.; Hänni, K. D.; Leigh, D. A.; Lusby, P. J.; Walker, D. B. *J. Am. Chem. Soc.* **2006**, *128* (7), 2186–2187.



- (52) Aucagne, V.; Berná, J.; Crowley, J. D.; Goldup, S. M.; Hänni, K. D.; Leigh, D. A.; Lusby, P. J.; Ronaldson, V. E.; Slawin, A. M. Z.; Viterisi, A.; Walker, D. B. J. *Am. Chem. Soc.* **2007**, *129* (39), 11950–11963.
- (53) Langton, M. J.; Xiong, Y.; Beer, P. D. *Chem. – Eur. J.* **2015**, *21* (52), 18910–18914.
- (54) Lim, J. Y. C.; Bunchuay, T.; Beer, P. D. *Chem. – Eur. J.* **2017**, *23* (19), 4700–4707.
- (55) Brotherton, W. S.; Clark, R. J.; Zhu, L. J. *Org. Chem.* **2012**, *77* (15), 6443–6455.
- (56) Zhou, E.; Zhang, J.; Dong, C. *ARKIVOC* **2014**, *v*, 351–364.
- (57) Parmar, D.; Sugiono, E.; Raja, S.; Rueping, M. *Chem. Rev.* **2014**, *114* (18), 9047–9153.
- (58) Hynes, M. J. J. *Chem. Soc. Dalton Trans.* **1993**, No. 2, 311–312.
- (59) Kim, S.-G.; Kim, K.-H.; Jung, J.; Shin, S. K.; Ahn, K. H. *J. Am. Chem. Soc.* **2002**, *124* (4), 591–596.
- (60) Zhang, X. X.; Bradshaw, J. S.; Izatt, R. M. *Chem. Rev.* **1997**, *97* (8), 3313–3362.
- (61) Interestingly, Sánchez and co-workers reported the preponderance of axial chirality over point chirality in the formation of homochiral supramolecular aggregates in Buendía, J.; Greciano, E. E.; Sánchez L. J. *Org. Chem.*, **2015**, *80* (24), 12444–12452.
- (62) Ufimtsev, I. S.; Martinez, T. J. J. *Chem. Theory Comput.* **2009**, *5* (10), 2619–2628.
- (63) Titov, A. V.; Ufimtsev, I. S.; Luehr, N.; Martinez, T. J. J. *Chem. Theory Comput.* **2013**, *9* (1), 213–221.
- (64) Song, C.; Wang, L.-P.; Martinez, T. J. J. *Chem. Theory Comput.* **2016**, *12* (1), 92–106.
- (65) Kästner, J.; Carr, J. M.; Keal, T. W.; Thiel, W.; Wander, A.; Sherwood, P. J. *Phys. Chem. A* **2009**, *113* (43), 11856–11865.
- (66) Goumans, T. P. M.; Catlow, C. R. A.; Brown, W. A.; Kästner, J.; Sherwood, P. *Phys. Chem. Chem. Phys.* **2009**, *11* (26), 5431.
- (67) Tomov, S.; Dongarra, J.; Baboulin, M. *Parallel Comput.* **2010**, *36* (5–6), 232–240.
- (68) Case, D. A.; Betz, R. M.; Botello-Smith, W.; Cerutti, D. S.; T.E. Cheatham, I.; Darden, T. A.; Duke, R. E.; Giese, T. J.; Gohlke, H.; Goetz, A. W.; Homeyer, N.; Izadi, S.; Janowski, P.; Kaus, J.; Kovalenko, A.; Lee, T. S.; LeGrand, S.; Li, P.; Lin, C.; Luchko, T.; Luo, R.; Madej, B.; Mermelstein, D.; Merz, K. M.; Monard, G.; Nguyen, H.; Nguyen, H. T.; Omelyan, I.; Onufriev, A.; Roe, D. R.; Roitberg, A.; Sagui, C.; Simmerling, C. L.; Swails, J.; Walker, R. C.; Wang, J.; Wolf, R. M.; Wu, X.; Xiao, L.; York, D. M.; Kollman, P. A. *AMBER 2016*; University of California: San Francisco, 2016.
- (69) Salomon-Ferrer, R.; Götz, A. W.; Poole, D.; Le Grand, S.; Walker, R. C. J. *Chem. Theory Comput.* **2013**, *9* (9), 3878–3888.
- (70) Le Grand, S.; Götz, A. W.; Walker, R. C. *Comput. Phys. Commun.* **2013**, *184* (2), 374–380.
- (71) Wang, J.; Wolf, R. M.; Caldwell, J. W.; Kollman, P. A.; Case, D. A. *J. Comput. Chem.* **2004**, *25* (9), 1157–1174.
- (72) Wang, J.; Wolf, R. M.; Caldwell, J. W.; Kollman, P. A.; Case, D. A. *J. Comput. Chem.* **2005**, *26* (1), 114–114.
- (73) Ibrahim, M. A. *J. Comput. Chem.* **2011**, *32* (12), 2564–2574.
- (74) Lang, D. A.; Mannesse, M. L. M.; De Haas, G. H.; Verheij, H. M.; Dijkstra, B. W. *Eur. J. Biochem.* **1998**, *254* (2), 333–340.
- (75) Morozov, A. N.; D’Cunha, C.; Alvarez, C. A.; Chatfield, D. C. *Biophys. J.* **100** (4), 1066–1075.
- (76) Müller, T. A.; Zavodszky, M. I.; Feig, M.; Kuhn, L. A.; Hausinger, R. P. *Protein Sci.* **2006**, *15* (6), 1356–1368.
- (77) Hoekman, S.; Kitching, M. O.; Leigh, D. A.; Papmeyer, M.; Roke, D. J. *Am. Chem. Soc.* **2015**, *137* (24), 7656–7659.
- (78) Blanco, V.; Leigh, D. A.; Marcos, V.; Morales-Serna, J. A.; Nussbaumer, A. L. J. *Am. Chem. Soc.* **2014**, *136* (13), 4905–4908.
- (79) Tachibana, Y.; Kihara, N.; Takata, T. J. *Am. Chem. Soc.* **2004**, *126* (11), 3438–3439.
- (80) Galli, M.; Lewis, J. E. M.; Goldup, S. M. *Angew. Chem. Int. Ed.* **2015**, *54* (46), 13545–13549.
- (81) Barat, R.; Legigan, T.; Tranoy-Opalinski, I.; Renoux, B.; Peraudeau, E.; Clarhaut, J.; Poinot, P.; Fernandes, A. E.; Aucagne, V.; Leigh, D. A.; Papot, S. *Chem Sci* **2015**, *6* (4), 2608–2613.
- (82) Carlone, A.; Goldup, S. M.; Lebrasseur, N.; Leigh, D. A.; Wilson, A. J. *Am. Chem. Soc.* **2012**, *134* (20), 8321–8323.
- (83) Lewandowski, B.; De Bo, G.; Ward, J. W.; Papmeyer, M.; Kuschel, S.; Aldegunde, M. J.; Gramlich, P. M. E.; Heckmann, D.; Goldup, S. M.; D’Souza, D. M.; Fernandes, A. E.; Leigh, D. A. *Science* **2013**, *339* (6116), 189.
- (84) Yang, W.; Li, Y.; Zhang, J.; Chen, N.; Chen, S.; Liu, H.; Li, Y. *Small* **2012**, *8* (16), 2602–2607.